CHIN. PHYS. LETT. Vol. 37, No. 8 (2020) 087505

Enhancement of Curie Temperature under Built-in Electric Field in Multi-Functional Janus Vanadium Dichalcogenides

Shilei Ji(季石磊), Hong Wu(武红), Shuang Zhou(周双), Wei Niu(钮伟), Lujun Wei(魏陆军), Xing-Ao Li(李兴鳌), Feng Li(李峰)*, and Yong Pu(普勇)*

New Energy Technology Engineering Laboratory of Jiangsu Provence & School of Science, Nanjing University of Posts and Telecommunications, Nanjing 210023, China

(Received 9 April 2020; accepted 27 May 2020; published online 28 July 2020)

Functionalized two-dimensional materials with multiferroicity are highly desired to be next-generation electronic devices. Here we theoretically predict a family of Janus vanadium dichalcogenides VXX' (X/X' = S, Se, Te) monolayers with multiferroic properties, combing ferromagnetism, ferroelasticity and piezoelectricity. Due to the unpaired electrons on the V atom, the Janus VXX' monolayers have intrinsic long-range ferromagnetic orders. Particularly, the Curie temperature of 1T-VSeTe monolayer is up to 100 K, which is greatly higher than 2D 1T-VSe_2 and 1T-VTe_2. Furthermore, the six Janus VXX' monolayers have similar crater-like ferroelastic switching curves. Compared to black phosphorus, 2H-VSSe monolayer has the similar ferroelastic switching signal and 4 times lower energy barrier. In addition, the out-of-plane piezoelectricity induced by the structure asymmetry in the vertical direction gives the 2H-VXX' monolayers the potential to be piezoelectric materials. It is found that a built-in electric field in the vertical direction due to the different electronegativity values of chalcogen atoms induces the changes of electronic structures, which leads to the appearance of three different types of band gaps in the three H-phase structures. Recently, the experimental growth of the Janus MoSSe monolayers and the electrochemical exfoliation of ferromagnetic monolayered VSe_2 make the Janus VXX' monolayers possibly fabricated in experiments.

PACS: 75.30.Kz, 75.85.+t, 77.55.Nv, 78.20.−e DOI: 10.1088/0256-307X/37/8/087505

Since the first one-atom-thick material graphene was discovered in 2004,[1] two-dimensional (2D) materials have attracted a great deal of attention. Among these 2D materials, transition-metal dichalcogenides (TMDs) have been widely studied for their excellent properties, including a wide range of energy bandgap, tunable electronic and optical properties, *etc.*[2] TMDs have the potential to be applied in the field of spintronics and high-performance sensors. In addition, functionalized 2D TMDs can generate new characteristics, for example, Li-exfoliated MoS_2 possesses enhanced catalytic activity.[3−10]

Multiferroic materials are considered as a special class of functional compounds with two or more ferroic properties, including ferromagnetism, ferroelasticity and ferroelectricity.[11,12] Coupling between different ferroic orderings can create new phenomena, which has great potential for applications in electronic devices.[11−15] For example, in $BiFeO_3$, the multiferroics can be induced by defect engineering or the magnetic proximity effect.[16] However, the coupling effect between different magnetic orderings is so weak, since the origins of the multiferroics are diverse from each other. Ferromagnetism originates mainly from unpaired electrons on partially filled d/f orbitals on transition metals, ferroelectricity is derived from empty d/f orbitals, while ferroelasticity originates from the lattice distortion. This means that ferroelectricity and ferromagnetism are derived from the space- and time-symmetry breakings, respectively, while ferroelasticity demands neither. Therefore, to date, there have been very few multiferroic materials that can be maintained at room temperature.

Recently in 2017, the first intrinsic ferromagnetic two-dimensional CrI_3 and $CrGeTe_3$ were successfully fabricated for the first time,[17,18] bringing the study of ferromagnetism from 3D down to 2D. The curie temperature (T_c) of the monolayered CrI_3 and $CrGeTe_3$ are 45 and 30 K, respectively. The virtual exchange between a half-occupied and an empty orbital in a super-exchange system results in the weak FM coupling, which makes a low Curie temperature in monolayered CrI_3 and $Cr_2Ge_2Te_6$.[19] After that, the Curie temperature is enhanced to 100 K found in three-layered Fe_3GeTe_2,[20] and further be modulated up to the room temperature. Very recently, monolayered VSe_2 is reported to have a high Curie temperature,[21−25] in which the T_c of electrochemical exfoliation 1T-VSe_2 monolayer even reaches up to 470 K (1 or 2 stands for how many layers in the unit cell, T stands for trigonal).[21] However, the absence of ferromagnetism in 1T-VSe_2 is still contro-

Supported by the National Natural Science Foundation of China (Grant Nos. 61704083, 61605087 and 61874060), the Natural Science Foundation of Jiangsu Province (Grant Nos. BK20160881 and BK20181388), and the Foundation of Nanjing University of Posts and Telecommunications (Grant No. NY219030).

*Corresponding author. Email: lifeng@njupt.edu.cn; puyong@njupt.edu.cn

© 2020 Chinese Physical Society and IOP Publishing Ltd

versial. Molecular beam epitaxial VSe_2 monolayer is found no long-range ferromagnetic order on highly oriented pyrolytic graphite substrates.[26,27] There could be two reasons for this being controversial: on the one hand, synthesis methods of VSe_2 sheets may affect the geometric structure, and thus further affect the ferromagnetic order; on the other hand, the charge-density-wave phase transition found in 1T-VSe_2 at low temperatures opens an energy band gap at the Fermi surface, resulting in the disappearance of the ferromagnetic ordering.[23,27,28] Recently, Wang *et al.* predicted the Curie temperature of GdI_2 monolayer to survive near room temperature, arousing intense discussion.[29]

In this letter, we predict a new family of multiferroic 2D materials of Janus VXX' (X/X' = S, Se, Te) monolayers. Firstly, contributed by the V $3d$ orbitals, Janus VXX' monolayers have intrinsic ferromagnetism. In particular, the computed T_c of 2H-VSeTe (H, hexagonal) is up to 150 K, which is higher than the other 2D ferromagnetic materials.[17,18,20] The enhancement of the Curie temperature is due to the built-in electric field effect, resulting from the distinct electronegativity of chalcogen atoms on both sides of the V layer. Secondly, piezoelectricity is found in Janus VXX' monolayers. Due to the different electronegativity values of chalcogen atoms on both sides of the V layer, net intrinsic electric field is formed in the vertical direction, thus V d, Se p and Te p orbitals significantly affect the energy levels of bands. This result is also confirmed by the analysis of partial density of states (PDOS). Thirdly, the reversible ferroelastic strains of 1T- and 2H-VSSe monolayer reach up to 73% and the overall ferroelastic switching energy barriers are 0.26 eV/atom, which is 4 times lower than black phosphorus (73%, 0.99 eV/atom).[30] In consequence, Janus vanadium dichalcogenides VXX' are multi-functional with intrinsic ferromagnetism, effective ferroelasticity and high piezoelectricity.

All first-principle calculations were performed within the frame of density functional theory (DFT) using the Vienna ab initio simulation package (VASP) based on the projected augmented wave (PAW) method[31–33] The electron configurations of V, S, Se and Te are $3p^6 3d^4 4s^1$, $3s^2 3p^4$, $4s^2 4p^4$ and $5s^2 5p^4$, respectively. The plane-wave cut-off energy was set to 450 eV and a k-point grid of $10 \times 10 \times 1$ was used. The force on each atom was smaller than 1 meV/Å. The Heyd–Scuseria–Ernzerhof hybrid functional (HSE06 method) was carried out on the calculation of band structure, partial density of states and piezoelectric polarization.[34] The 'Berry phase' theory was used in the piezoelectric polarization calculations (LCALCPOL = TRUE).[35,36] The phonon-dispersion relations was calculated by employing the density-functional perturbation theory (DFPT) and PHONOPY,[37] and a $2 \times 2 \times 1$ supercell was applied in the DFPT calculations. The nudged-elastic-band (NEB) method was used in the ferroelastic calculation. The Mcsolver software was used in the Monte Carlo simulations.[38] A 16×16 lattice was used for all the simulations. In the piezoelectric polarization calculations, a uniaxial strain was applied along the armchair direction of the orthorhombic supercell (Fig. 1), the constant of zigzag direction and the atom positions were totally relaxed.

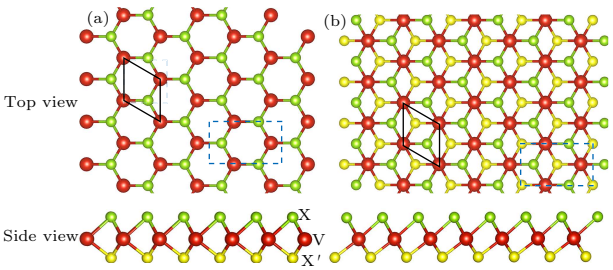

Fig. 1. The atomic structure of the (a) 2H- and (b) 1T-VXX' (X/X' = S, Se, Te). The hexagonal primitive cells and the orthorhombic supercells are labeled in black solid lines and blue dashed lines.

As is shown in Fig. 1, Janus VXX' monolayers consist of a layer of V atoms sandwiched between two different chalcogen atoms (S, Se and Te). Janus VXX' monolayers have 1T and 2H phases. The monolayered 2H-Janus VXX' is an ABA stack, while the monolayered 1T-Janus VXX' is an ABC stack. Table S1 and Fig. S1 in the supplementary material shows the lattice constant, bond length, bond angle of the Janus VXX' monolayers. The constants of 2H-VS_2, 2H-VSe_2 and 2H-VSSe are consistent with the previous theoretical reports.[39,40] The lattice constant of Janus monolayered VXX' is between those of monolayered VX_2 and VX'_2. In addition, we find that as the number of electrons increases, the bond length and lattice constant also change from small to large in turn. Because of the different chalcogen atoms on both sides, the Janus monolayered VXX' has the space-inversion symmetry in vertical direction. The phonon spectrum calculations of all VXX' monolayers shown in Fig. S2 indicate that they are all dynamically stable and can exist as freestanding 2D monolayers.

Figure 2 shows the band structures of 2H and 1T Janus monolayered VXX'. In order to accurately calculate the electronic structures of the Janus vanadium dichalcogenides, we decide to use the Heyd–Scuseria–Ernzerhof hybrid functional (HSE06) method. All of the three 2H-VXX' monolayers are indirect semiconductors, while the 1T-VXX' is metal. In Fig. 2(a), the 2H-VSSe monolayer has a band gap of 1.01 eV. The spin-down (red) and spin-up (black) band gaps are 1.47 eV and 1.01 eV, respectively. The valence band maximum (VBM) and the conduction band minimum (CBM) are both spin-up bands. Based on the PDOS in Fig. 3(a), we can conclude that V d_{z^2} and S p_x orbitals contribute to the VBM in VSSe, and V d_{z^2} orbital also contributes to the CBM in VSSe.

In Fig. 2(b), 2H-VSeTe has a band gap of 0.47 eV, which is smaller than that of 2H-VSSe. The spin-up

and spin-down gaps are 0.87 eV and 0.88 eV. In contrast to the 2H-VSSe, 2H-VSeTe has a staggered band gap: the VBM is the spin-down band located at the Γ point, while the CBM is the spin-up band located at the K point. Meanwhile, the VBM and CBM are separately contributed by spin-up and spin-down electrons. The valence bands and conductive bands shift down simultaneously. Based on the PDOS in Fig. 3(b), we conclude that the VBM is contributed by V d_{xy}, d_{yz}, d_{yz}, $d_{x^2-y^2}$ and Te p_x, p_y orbitals, while the CBM is contributed by V d_{z^2} orbital. In contrast to the 2H-VSTe [Fig. 3(c)], the spin-up band near the Fermi level in 2H-VSeTe is contributed by V d_{z^2} and Se p_z orbitals, which opens the spin-up band gap.

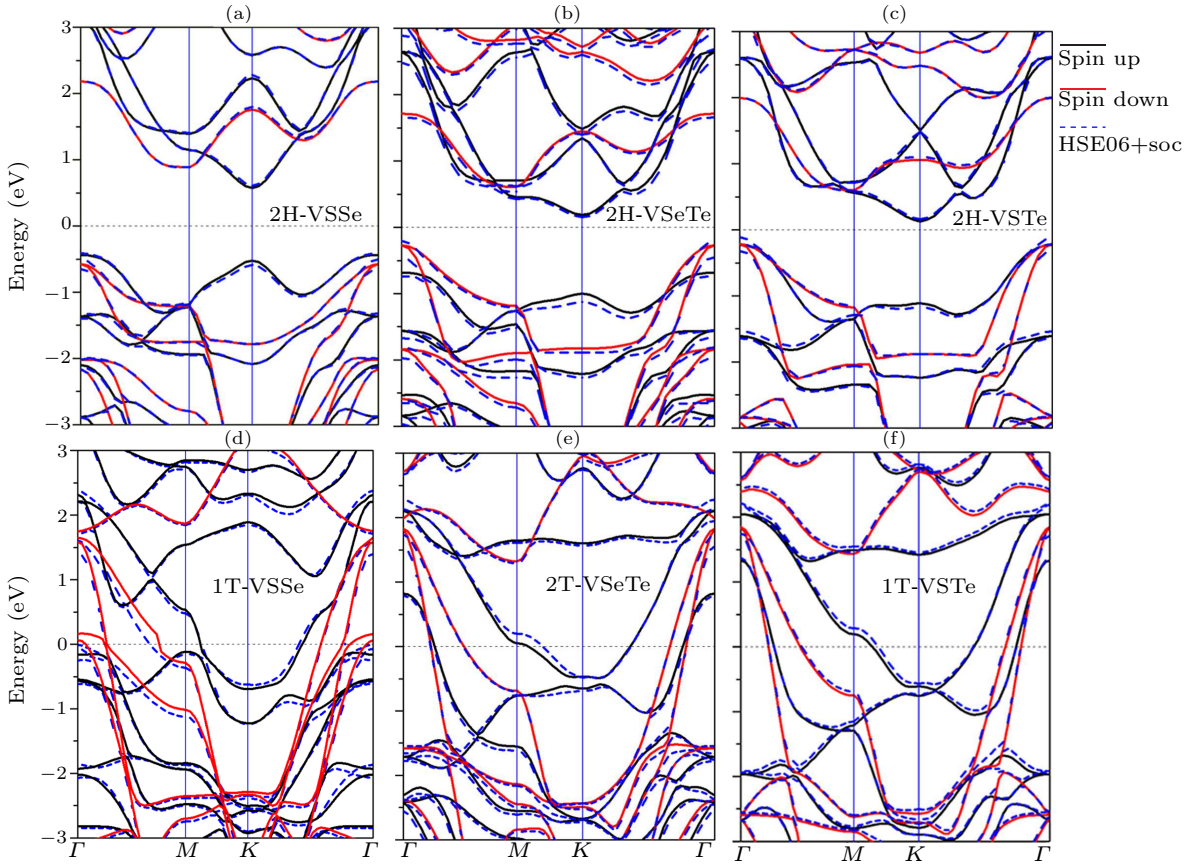

Fig. 2. The band structure of 2H (a) VSSe, (b) VSeTe, (c) VSTe and 1T (d) VSSe, (e) VSeTe, (f) VSTe. The red lines represent spin-down bands, the dark lines represent spin-up bands, and the blue dotted lines represent the band structure with the SOC and HSE06 method. The Fermi level is set to zero.

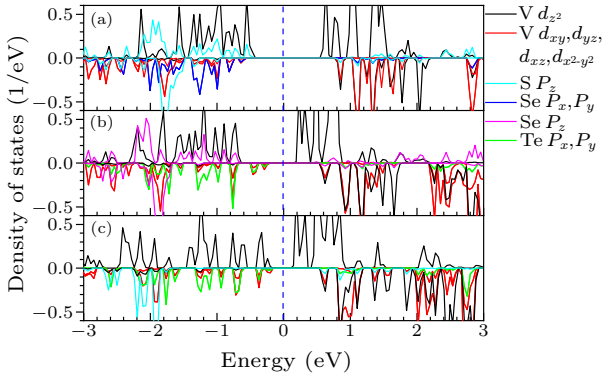

Fig. 3. The partial density of states (PDOS) of 2H (a) VSSe, (b) VSeTe, (c) VSTe. The Fermi level is set to zero.

Figure 2(c) shows the band structure of 2H-VSTe without and with SOC. The band gap of 2H-VSTe is 0.36 eV, which is smaller than 2H-VSSe and 2H-VSeTe. The spin-up and spin-down gaps are 0.36 eV and 0.82 eV. Here 2H-VSTe has a flat band-gap: the CBM, located at the K point, is the spin-up band contributed by V d_{z^2} orbital, while the VBM, located at Γ point, is composed of spin-up and spin-down bands, which is contributed by V d_{z^2} orbital and V d_{xy}, d_{yz}, d_{xz}, $d_{x^2-y^2}$, Te p_y, p_x orbitals, respectively. Due to the contribution of V d_{xy}, d_{yz}, d_{yz}, $d_{x^2-y^2}$ and Te p_x, p_y orbitals, 2H-VSeTe and 2H-VSTe have the similar energy level in spin-down bands.

Based on the band structure and PDOS analysis of the Janus monolayered VXX', different electronegativity values of chalcogen atoms greatly affect the both spin-up and spin-down bands. Obviously, the 2H-VSSe is the nested band-gap contributed by V d and S p orbitals, while 2H-VSeTe and 2H-VSTe are staggered band gap and flat band gap, respectively, contributed by V d and Te p orbitals.

It can be noticed from the band structure and PDOS that the spin-up and spin-down bands of VXX'

are separate, which represents the ferromagnetism order in VXX' monolayers. Then we turned to confirm the ferromagnetism order at higher temperature. The Curie temperature T_c can determine how high temperature the ferromagnetic material can remain in ferromagnetism order. Based on the magnetic anisotropy energy (MAE) calculation (Table S3), the MAE of monolayered 2H-VSeTe reaches -1.094 meV/V atom. We decide to use the Monte Carlo simulations with the Ising model to calculate the Curie temperatures. The Hamiltonian of the Ising model is

$$H = -\sum_{i,j} J \cdot \boldsymbol{s}_i \cdot \boldsymbol{s}_j,$$

where J is the exchange coupling constant, $\boldsymbol{s}$ is the spin of the V atom. The Curie temperature of CrI_3 calculated by Monte Carlo simulations with the Ising model is 60 K, which is close to the experimental result (Fig. S3).[41] As shown in Fig. 4, based on the PBE method, the Curie temperature of 2H-VSeTe monolayer is ∼150 K, which is far higher than the temperature of liquid nitrogen (77 K), indicating that 2H-VSeTe monolayer can maintain ferromagnetic order in liquid nitrogen environment. Meanwhile, the Curie temperature of 1T-VSeTe is much higher than those of 1T-VSe_2 and 1T-VTe_2. The electronegativity of chalcogen atoms greatly affects the exchange coupling constants (Table S2), resulting in the enhancement of Curie temperature in Janus VXX' monolayers. Although the Curie temperatures of VXX' monolayers are lower than room temperature, T_c's of 2H-VSSe (∼100 K), VSeTe (∼150 K), VSTe (∼100 K) and 1T-VSeTe (∼100 K), VSTe (∼80 K) are still higher than those of CrI_3 and $CrGeTe_3$ monolayers,[17,18] indicating that monolayered VXX' materials are promising ultrathin nanomaterials for potential applications in spintronics.

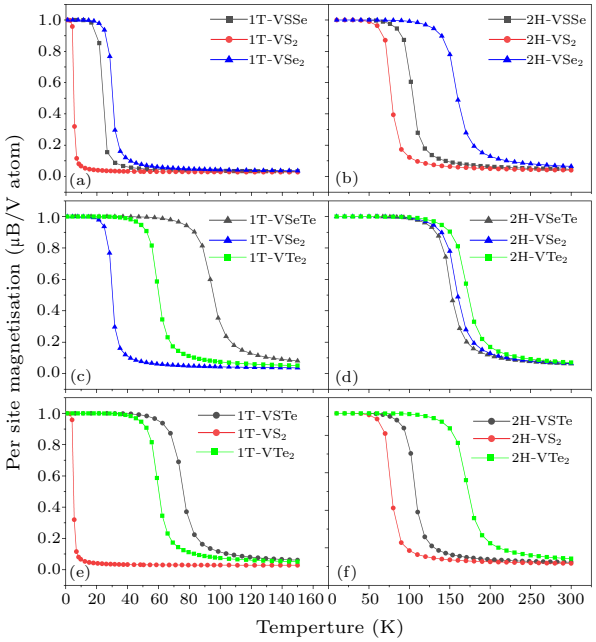

Fig. 4. Per site magnetization of [(a), (c), (e)] 1T and [(b), (d), (f)] 2H-VXX' monolayers as a function of temperature. Black squares, black triangles and black circles denote VSSe, VSeTe and VSTe, respectively. Red circles, blue triangles and green squares stand for VS_2, VSe_2 and VTe_2, respectively. The Curie temperatures of 2H-VSSe, 2H-VSeTe and 2H-VSTe are ∼100 K, ∼150 K and ∼100 K, respectively. Meanwhile, the Curie temperatures of 1T-VSSe, 1T-VSeTe and 1T-VSTe are ∼25 K, ∼75 K and ∼100 K, respectively.

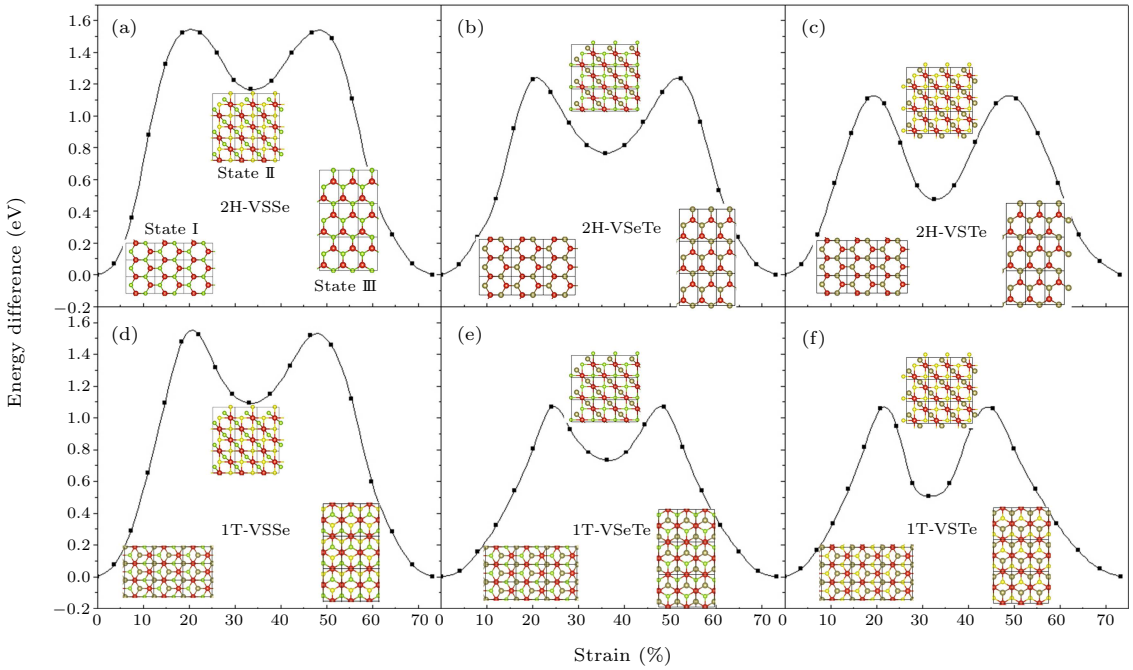

Fig. 5. The curve between the uniaxial strain and the energy difference of 2H (a) VSSe, (b) VSeTe, (c) VSTe and 1T (d) VSSe, (e) VSeTe, (f) VSTe. The pathway of the NEB method is shown in (a), state I is the initial state, state Ⅱ is the intermediate state and state Ⅲ is the final state. Red, yellow, green and brown balls denote V, S, Se and Te atoms, respectively.

Since the 2D-VXX' unit cells are all rhombic, we have chosen a rectangular supercell [Fig. 5(a)]. Compared with the rhombic unit cell, the orthorhombic supercell contains six atoms, which form a hexagon (Fig. 1). State I define the directions along armchair and zigzag as a and b. The lattice constant a along the armchair direction is larger than b along the zigzag direction. In Fig. 5(a), state Ⅱ is the intermediate state of square unit cell. In order to obtain an accurate intermediate structure, we first use the method of molecular thermodynamics to generate a square unit cell with a lattice constant of $a' = b'$ at a constant temperature of 1000 K for 2 ps, and then perform structural optimization. State Ⅲ can be regarded as the structure in which state I is rotated by 90°, the reversible ferroelastic switching strain is defined as $(\frac{b}{a} - 1) \times 100\%$.

In order to explore the evolution of configuration under uniaxial strain, the energy as a function of the uniaxial strain was calculated by the NEB method,[42] as shown in Figs. 5(a)–5(f). Outstandingly, an impressive high reversible stress 73% for the ferroelastic switching is observed for 2H-VSSe monolayer. In the starting state I and the end state Ⅲ, three S/Se/Te atoms are bonded with the interlayer V atoms, respectively; while in the transition state Ⅱ, opposite trends are found for the S–V and Se–V bonds: the bond length of S–V is increased from 2.35 to 2.40 Å, while that of Se–V is decreased from 2.51 to 2.48 Å. As a whole, the configuration energy first increases by 0.26 eV/atom, then drops by 0.07 eV/atom. Similarly, under further stress, the configuration changes from state Ⅱ to Ⅲ. Overall, a significant ferroelastic switching effect is found in the VSSe monolayer with a moderate energy barrier of 0.26 eV/atom and a very large reversible ferroelastic strain of 73%, which is 4 times smaller than black phosphorus (73%, 0.99 eV/atom),[30] and much higher than those in other classical ferroelastic materials (0.5%–3%).[43,44] For other Janus VXX' monolayers, the energy barrier and ferroelastic strain are similar to the 2H-VSSe monolayer. Thus, Janus VXX' monolayers are suggested to produce stronger ferroelastic switching signals than phosphorene, which is crucial for designing sensors and data-storage devices.[44]

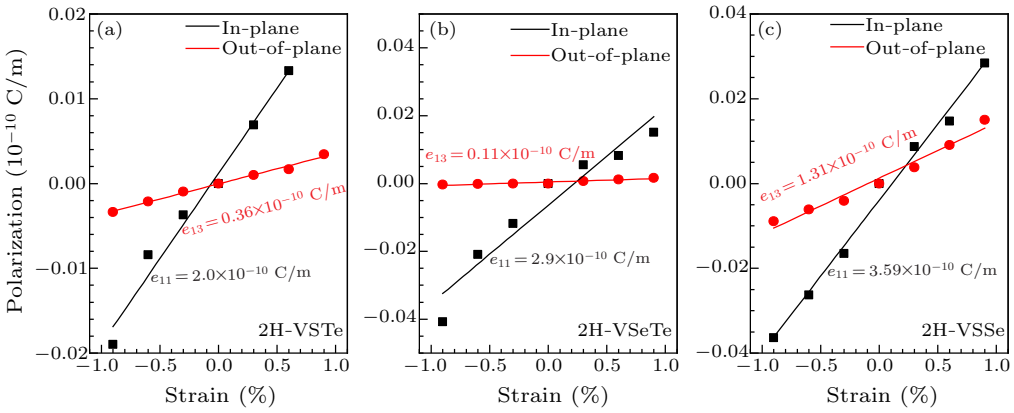

Fig. 6. The piezoelectric polarization of (a) VSTe, (b) VSeTe, (c) VSSe. The piezoelectric coefficients are calculated by applying a uniaxial strain along the armchair direction. In our calculations, the in-plane and out-of-plane piezoelectric coefficients of 2H-VSSe are close to previous calculations (in-plane: 3.303×10^{-10} C/m, out-of-plane: 0.948×10^{-10} C/m).[40]

The third-rank piezoelectric tensor is $e_{ijk} = \partial P_i / \partial \varepsilon_{jk}$, where P is electrical polarization and ε is strain. In order to accurately calculate the electrical polarization, we decide to use the Heyd–Scuseria–Ernzerhof hybrid functional (HSE06 method) to apply a uniaxial strain along the armchair direction of the orthorhombic supercells. As shown in Fig. 6, like other TMDs, Janus 2H-VXX' monolayers have the in-plane piezoelectric coefficients. The in-plane piezoelectric coefficients e_{11} of the Janus monolayered 2H-VSSe, VSeTe and VSTe are 3.59×10^{-10}, 2.9×10^{-10} and 2.0×10^{-10} C/m, respectively. The in-plane piezoelectric coefficient e_{11} of the Janus 2H-VSeTe monolayer is equal to MoS_2 monolayer (2.9×10^{-10} C/m).[45,46]

In contrast to monolayered MoS_2, 2H-VXX' monolayers have the intrinsic out-of-plane piezoelectricity in the out-of-plane direction since the different chalcogen atoms on both sides of the V atom on Janus 2H-VXX' monolayers, forming the built-in intrinsic electric field, break the space-inversion symmetry. The out-of-plane piezoelectric coefficients e_{13} of the VSSe, VSeTe and VSTe monolayers are calculated to be 1.31×10^{-10} C/m, 0.11×10^{-10} C/m and 0.36×10^{-10} C/m, respectively. Although the out-of-plane piezoelectric coefficients e_{13} of VSSe, VSeTe and VSTe are slightly smaller than the in-plane piezoelectric coefficients, 2D materials which have the out-of-plane piezoelectric coefficient e_{13} are scare. Furthermore, as a piezoelectric material, it is easier to measure the out-of-plane piezoelectric polarization by applying in-plane strain in the experiment.

In summary, we have predicted a class of multiferroic Janus VXX' (X/X' = S, Se, Te) monolayers with ferromagnetism, ferroelasticity and piezoelectricity. The high Curie temperature of 2H-VSeTe reaches 150 K, which is higher than 2D ferromagnetic mate-

rials in the experiments. The built-in electric field effect, resulting from the distinct electronegativity of chalcogen atoms on both the sides of the V layer, enhances the curie temperature of Janus 1T-VXX' monolayers. Compared to other classical ferroelastic materials (0.5–3%), the reversible ferroelastic strain of 73% makes VXX' monolayers have potential applications in sensors and data-storage devices. In addition, due to the space-inversion symmetry, 2H-VXX' monolayers have the out-of-plane and in-plane piezoelectricity, indicating that 2H-VXX' monolayers can be piezoelectric sensors in the future. Furthermore, due to different electronegativity values of S, Se, Te atoms, the Janus 2H-VXX' monolayers have three types of band gaps. The Janus VXX' monolayers calculated by first-principles have many attractive properties, we hope that this study will facilitate further experimental work in this field.

References

[1] Novoselov K S, Geim A K, Morozov S V, Jiang D, Zhang Y, Dubonos S V, Grigorieva I V and Firsov A A 2004 *Science* **306** 666
[2] Hu H, Zavabeti A, Quan H, Zhu W, Wei H, Chen D and Ou J Z 2019 *Biosens. Bioelectron.* **142** 111573
[3] Nair R R, Tsai I L, Sepioni M, Lehtinen O, Keinonen J, Krasheninnikov A V, Castro Neto A H, Katsnelson M I, Geim A K and Grigorieva I V 2013 *Nat. Commun.* **4** 2010
[4] McCreary K M, Swartz A G, Han W, Fabian J and Kawakami R K 2012 *Phys. Rev. Lett.* **109** 186604
[5] Ugeda M M, Brihuega I, Guinea F and Gomez-Rodriguez J M 2010 *Phys. Rev. Lett.* **104** 096804
[6] Červenka J, Katsnelson M I and Flipse C F J 2009 *Nat. Phys.* **5** 840
[7] Uchoa B, Kotov V N, Peres N M and Castro Neto A H 2008 *Phys. Rev. Lett.* **101** 026805
[8] Yazyev O V and Helm L 2007 *Phys. Rev. B* **75** 125408
[9] Chhowalla M, Shin H S, Eda G, Li L J, Loh K P and Zhang H 2013 *Nat. Chem.* **5** 263
[10] Choi Y H, Kwon G H, Jeong J H, Jeong K S, Kwon H, An Y, Kim M, Kim H, Yi Y, Im S and Cho M H 2019 *Appl. Surf. Sci.* **494** 37
[11] Huang W, Yin Y and Li X 2018 *Appl. Phys. Rev.* **5** 041110
[12] Hu T and Kan E 2019 *Wiley Interdisciplinary Rev.: Comput. Mol. Sci.* **9** e1409
[13] Gong C, Kim E M, Wang Y, Lee G and Zhang X 2019 *Nat. Commun.* **10** 2657
[14] Sun W, Wang W, Chen D, Cheng Z and Wang Y 2019 *Nanoscale* **11** 9931
[15] Zhang F, Mi W and Wang X 2019 *Nanoscale* **11** 10329
[16] Wang Z, Tang C, Sachs R, Barlas Y and Shi J 2015 *Phys. Rev. Lett.* **114** 016603
[17] Huang B, Clark G, Navarro-Moratalla E, Klein D R, Cheng R, Seyler K L, Zhong D, Schmidgall E, McGuire M A, Cobden D H, Yao W, Xiao D, Jarillo-Herrero P and Xu X D 2017 *Nature* **546** 270
[18] Gong C, Li L, Li Z, Ji H, Stern A, Xia Y, Cao T, Bao W, Wang C, Wang Y, Qiu Z Q, Cava R J, Louie S G, Xia J and Zhang X 2017 *Nature* **546** 265
[19] Huang C, Feng J, Wu F, Ahmed D, Huang B, Xiang H, Deng K and Kan E 2018 *J. Am. Chem. Soc.* **140** 11519
[20] Deng Y, Yu Y, Song Y, Zhang J, Wang N Z, Sun Z, Yi Y, Wu Y Z, Wu S, Zhu J, Wang J, Chen X H and Zhang Y 2018 *Nature* **563** 94
[21] Yu W, Li J, Herng T S, Wang Z, Zhao X, Chi X, Fu W, Abdelwahab I, Zhou J, Dan J, Chen Z, Chen Z, Li Z, Lu J, Pennycook S J, Feng Y P, Ding J and Loh K P 2019 *Adv. Mater.* **31** 1903779
[22] Zhou J, Qiao J, Duan C G, Bournel A, Wang K L and Zhao W 2019 *ACS Appl. Mater. & Interfaces* **11** 17647
[23] Esters M, Hennig R G and Johnson D C 2017 *Phys. Rev. B* **96** 235147
[24] Bonilla M, Kolekar S, Ma Y, Diaz H C, Kalappattil V, Das R, Eggers T, Gutierrez H R, Phan M H and Batzill M 2018 *Nat. Nanotechnol.* **13** 289
[25] Feng S and Mi W 2018 *Appl. Surf. Sci.* **458** 191
[26] Zhang W, Zhang L, Wong P K J, Yuan J, Vinai G, Torelli P, van der Laan G, Feng Y P and Wee A T S 2019 *ACS Nano* **13** 8997
[27] Coelho P M, Nguyen Cong K, Bonilla M, Kolekar S, Phan M H, Avila J, Asensio M C, Oleynik I I and Batzill M 2019 *J. Phys. Chem. C* **123** 14089
[28] Chen P, Pai W W, Chan Y H, Madhavan V, Chou M Y, Mo S K, Fedorov A V and Chiang T C 2018 *Phys. Rev. Lett.* **121** 196402
[29] Wang B, Zhang X, Zhang Y, Yuan S, Guo Y, Dong S and Wang J 2020 *Mater. Horiz.* **7** 1623
[30] Tu Z and Wu M 2020 *Sci. Bull.* **65** 147
[31] Kresse G and Joubert D 1999 *Phys. Rev. B* **59** 1758
[32] Kresse G and Furthmuller J 1996 *Phys. Rev. B* **54** 11169
[33] Blochl P E 1994 *Phys. Rev. B* **50** 17953
[34] Heyd J, Scuseria G E and Ernzerhof M 2003 *J. Chem. Phys.* **118** 8207
[35] King-Smith R D and Vanderbilt D 1993 *Phys. Rev. B* **47** 1651
[36] Vanderbilt D 2000 *J. Phys. Chem. Solids* **61** 147
[37] Togo A and Tanaka I 2015 *Scr. Mater.* **108** 1
[38] Liu L, Ren X, Xie J, Cheng B, Liu W, An T, Qin H and Hu J 2019 *Appl. Surf. Sci.* **480** 300
[39] Yang J, Wang A, Zhang S, Liu J, Zhong Z and Chen L 2019 *Phys. Chem. Chem. Phys.* **21** 132
[40] Zhang C, Nie Y, Sanvito S and Du A 2019 *Nano Lett.* **19** 1366
[41] Lado J L, Fernández-Rossier J 2017 *2D Mater.* **4** 035002
[42] Xu X, Ma Y, Huang B and Dai Y 2019 *Phys. Chem. Chem. Phys.* **21** 7440
[43] Salje E K H 2012 *Annu. Rev. Mater. Res.* **42** 265
[44] Wang C, Ke X, Wang J, Liang R, Luo Z, Tian Y, Yi D, Zhang Q, Wang J, Han X F, Van Tendeloo G, Chen L Q, Nan C W, Ramesh R and Zhang J 2016 *Nat. Commun.* **7** 10636
[45] Zhu H, Wang Y, Xiao J, Liu M, Xiong S, Wong Z J, Ye Z, Ye Y, Yin X and Zhang X 2015 *Nat. Nanotechnol.* **10** 151
[46] Wu W, Wang L, Li Y, Zhang F, Lin L, Niu S, Chenet D, Zhang X, Hao Y, Heinz T F, Hone J and Wang Z L 2014 *Nature* **514** 470

supplementary material

Enhancement of Curie temperature under built-in electric field in Multi-functional Janus vanadium dichalcogenides

Shilei Ji(季石磊), Hong Wu(武红), Shuang Zhou(周双), Wei Niu(钮伟), Lujun Wei(魏陆军), Xing'ao Li(李兴鳌)[**], *Feng Li(李峰)*[**], *Yong Pu(普勇)*[**]

[1]*New Energy Technology Engineering Laboratory of Jiangsu Provence & School of Science, Nanjing University of Posts and Telecommunications (NJUPT), Nanjing 210023, China*

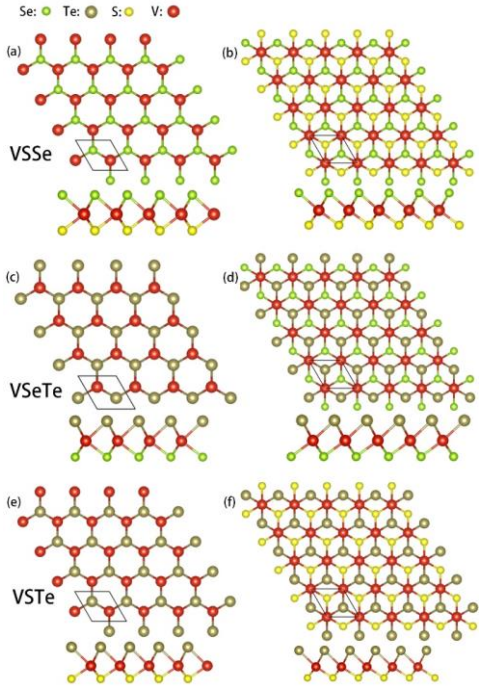

Fig. S1. The atomic structures of the 2H- (a) VSSe, (c) VSeTe, (e) VSTe and 1T- (b) VSSe, (d) VSeTe, (f) VSTe monolayers. The hexagonal primitive cells are labeled in dark solid lines. The red, yellow, green and brown balls are V, S, Se and Te atoms, respectively.

Table S1. The lattice constant, bond length, bond angle of the Janus VXX' monolayers.

	Lattice (Å)	V– S (Å)	V– Se (Å)	V– Te (Å)	V– S– V (deg)	V– Se– V (deg)	V– Te– V (deg)
2H-VS_2	3.17	2.36	—	—	84.34	—	—
2H-VSe_2	3.33	—	2.50	—	—	83.52	—
2H-VTe_2	3.57	—	—	2.72	—	—	82.14
2H-VSSe	3.25	2.35	2.51	—	87.26	80.69	—
2H-VSeTe	3.45	—	2.50	2.72	—	87.43	78.86
2H-VSTe	3.37	2.35	—	2.71	91.62	—	76.75
1T-VS_2	3.18	2.35	—	—	84.79	—	—
1T-VSe_2	3.34	—	2.49	—	—	83.99	—
1T-VTe_2	3.56	—	—	2.71	—	—	81.86
1T-VSSe	3.27	2.35	2.50	—	88.21	81.39	—
1T-VSeTe	3.46	—	2.48	2.72	—	88.14	78.96
1T-VSTe	3.41	2.34	—	2.73	93.36	—	77.07

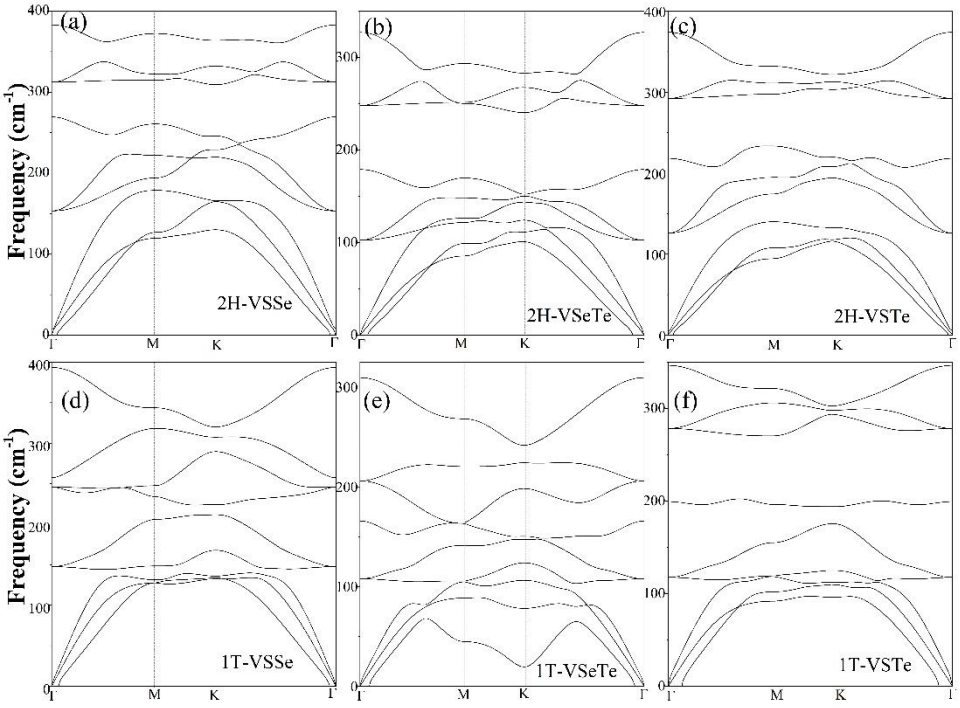

Fig. S2. The phonon spectrum calculations for the six Janus-VXX'. It can be clearly seen that the phonon spectra of the six Janus-VXX' have no imaginary frequency, indicating that they are all dynamically stable and they can exist as free-standing 2D monolayers. Very recently, the Janus MoSSe monolayer has been successfully synthesized. The H_2 is passed into the chamber with MoS_2 to strip and replace the top-layer S atom, and then the Se powder is thermally evaporated to replace the H atom to synthesize the Janus MoSSe monolayer.[1] We believe that the Janus VXX' monolayers can also be prepared in the same way.

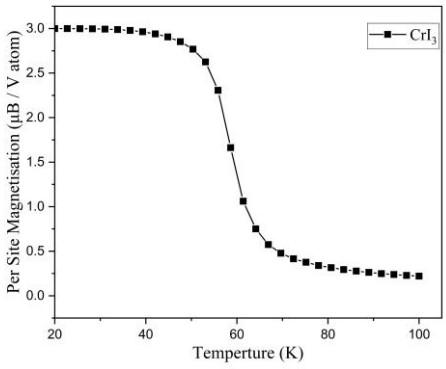

Fig. S3. Per site magnetization of CrI_3 monolayer as a function of temperature. The dark squares are the Monte Carlo simulations. T_c based on our calculation for CrI_3 monolayer is 60 K, which agrees with the experimental result 45 K [2].

Table S2. The exchange coupling constants (J) of 1T- and 2H- VXX' monolayers.

	J (meV)		**J (meV)**
1T-VSSe	-5.17	2H-VSSe	-22.62
1T-VSeTe	-20.78	2H-VSeTe	-33.24
1T-VSTe	-16.49	2H-VSTe	-23.34

1T-VS_2	-1.15	2H-VS_2	-17.00
1T-VSe_2	-6.54	2H-VSe_2	-34.79
1T-VTe_2	-13.1	2H-VTe_2	-37.58

Table S3. The magnetic anisotropy energy of 1T- and 2H- VXX' monolayers.

	$E_{in\text{-}plane} - E_{out\text{-}of\text{-}plane}$ (meV / V atom)	
	1T	2H
VSSe	0.052	-0.413
VSeTe	-0.171	-1.094
VSTe	-0.520	-0.768

References

[1] Lu A Y, Zhu H, Xiao J, Chuu C P, Han Y, Chiu M H, Cheng C C, Yang C W, Wei K H, Yang Y, Wang Y, Sokaras D, Nordlund D, Yang P, Muller D A, Chou M Y, Zhang X and Li L J 2017 *Nat Nanotechnol* **12** 744-749.

[2] Huang B, Clark G, Navarro-Moratalla E, Klein D R, Cheng R, Seyler K L, Zhong D, Schmidgall E, McGuire M A, Cobden D H, Yao W, Xiao D, Jarillo-Herrero P and Xu X 2017 *Nature* **546** 270-273.